

9. N. Myers, J. Kent, *Proc. Natl. Acad. Sci. U.S.A.* **100**, 4963 (2003).
10. J. Bongaarts, *Popul. Dev. Rev.* **22**, 483 (1996).
11. FAO, *Global Forest Resources Assessment 2000: Main Report*, FAO Forestry Paper 140 (FAO, Rome, 2001).
12. J. Loh *et al.*, *Living Planet Report 2002* (WWF, Gland, Switzerland, 2002), available at www.panda.org/downloads/general/LPR_2002.pdf.
13. M. Jenkins, R. E. Green, J. Madden, *Conserv. Biol.* **17**, 20 (2003).
14. IUCN Species Survival Commission, *IUCN Red List Categories and Criteria, Version 3.1* (IUCN, Gland, Switzerland, 2001).
15. A. Estrada, R. Coates-Estrada, D. A. Meritt Jr., *Biodiversity Conserv.* **6**, 19 (1997).
16. A. Estrada, R. Coates-Estrada, A. A. Dadda, P. Cammarano, *J. Trop. Ecol.* **14**, 577 (1998).
17. D. J. Pain, M. W. Pienkowski, *Farming and Birds in Europe: The Common Agricultural Policy and Its Implications for Bird Conservation* (Academic Press, London, 1997).
18. G. C. Daily, *Nature* **411**, 245 (2001).
19. M. L. Rosenzweig, *Win-Win Ecology: How the Earth's Species Can Survive in the Midst of Human Enterprise* (Oxford Univ. Press, Oxford, 2003).
20. M. L. Rosenzweig, *Oryx* **37**, 194 (2003).
21. J. R. Krebs, J. D. Wilson, R. B. Bradbury, G. M. Siriwardena, *Nature* **400**, 611 (1999).
22. P. F. Donald, R. E. Green, M. F. Heath, *Proc. R. Soc. Lond. B. Biol. Sci.* **268**, 25 (2001).
23. European Environment Agency, *Environmental Signals 2002, Benchmarking the Millennium*, Environmental Assess-
- ment Report No. 9 (Office for Official Publications of the European Communities, Copenhagen, Denmark, 2002) available at http://reports.eea.eu.int/environmental_assessment_report_2002_9/en/sig02LOW.pdf.
24. J. A. McNeely, S. J. Scherr, *Ecoagriculture: Strategies to Feed the World and Save Wild Biodiversity* (Island Press, Washington, DC, 2002).
25. J. G. Robinson, *Int. Wildl.* **24**, 30 (1994).
26. P. F. Donald, *Conserv. Biol.* **18**, 17 (2004).
27. D. Southgate, in *The Causes of Tropical Deforestation: the Economic and Statistical Analysis of Factors Giving Rise to the Loss of Tropical Forests*, K. Brown, D. W. Pearce, Eds. (UCL Press, London, 1994), pp. 134–143.
28. P. E. Waggoner, *Technol. Soc.* **17**, 17 (1995).
29. D. T. Avery, *Issues Sci. Technol.* **14**, 59 (1997).
30. E. B. Barbier, J. C. Burgess, *Land Econ.* **73**, 174 (1997).
31. A. Angelsen, D. Kaimowitz, in *Tradeoffs or Synergies? Agricultural Intensification, Economic Development and the Environment*, D. R. Lee, C. B. Barrett, Eds. (CABI, Wallingford, UK, 2001), pp. 89–114.
32. D. R. Lee, C. B. Barrett, Eds., *Tradeoffs or Synergies? Agricultural Intensification, Economic Development and the Environment* (CABI, Wallingford, UK, 2001).
33. N. E. Borlaug, *In Vitro Cell. Dev. Biol.-Plant.* **38**, 221 (2002).
34. I. M. Goklany, M. W. Sprague, *Sustaining Development and Biodiversity: Productivity, Efficiency and Conservation* (Cato Institute, Washington, DC, 1992).
35. P. E. Waggoner, J. H. Ausubel, I. K. Wernick, *Popul. Dev. Rev.* **22**, 531 (1996).
36. C. D. Thomas *et al.*, *Nature* **427**, 145 (2004).

37. J. N. Pretty, *Agri-culture: Reconnecting People, Land and Nature* (Earthscan, London, 2002).

38. M. S. Freudenberg, K. S. Freudenberg, in *Natural Resources Management in African Agriculture: Understanding and Improving Current Practices*, F. P. C. B. Barrett, A. A. Aboud, Eds. (CABI, Wallingford, UK, 2002), pp. 181–192.

39. D. Kleijn, W. J. Sutherland, *J. Appl. Ecol.* **40**, 947 (2003).

40. J. B. Hughes, G. C. Daily, P. R. Ehrlich, *Ecol. Lett.* **5**, 121 (2002).

41. RSPB, *Futurescapes: Large-Scale Habitat Restoration for Wildlife and People* (Royal Society for the Protection of Birds, Sandy, UK, 2001).

42. M. Avery, *Ecos* **22**, 3 (2001).

43. W. J. Sutherland, *Trends Ecol. Evol.* **17**, 148 (2002).

44. We thank M. Avery, J. Brashares, T. Brooks, G. Daily, D. Gibbons, and B. Grenfell for discussion and A. Stattersfield, M. Sneary, and M. Balman for access to the World Bird Database. S.J.C. acknowledges funding from the Wellcome Trust.

Supporting Online Material

www.sciencemag.org/cgi/content/full/1106049/DC1

Materials and Methods

SOM Text

Figs. S1 and S2

Table S1

References

5 October 2004; accepted 30 November 2004

Published online 23 December 2004;

10.1126/science.1106049

Include this information when citing this paper.

REPORTS

Ammonia Synthesis from First-Principles Calculations

K. Honkala,^{1,2} A. Hellman,⁴ I. N. Remediakis,^{1,2} A. Logadottir,^{1,2}
A. Carlsson,⁴ S. Dahl,⁴ C. H. Christensen,^{1,3} J. K. Nørskov^{1,2*}

The rate of ammonia synthesis over a nanoparticle ruthenium catalyst can be calculated directly on the basis of a quantum chemical treatment of the problem using density functional theory. We compared the results to measured rates over a ruthenium catalyst supported on magnesium aluminum spinel. When the size distribution of ruthenium particles measured by transmission electron microscopy was used as the link between the catalyst material and the theoretical treatment, the calculated rate was within a factor of 3 to 20 of the experimental rate. This offers hope for computer-based methods in the search for catalysts.

Detailed theoretical descriptions of the way in which solid surfaces act as catalysts for chemical reactions are now being obtained from density functional theory (DFT) calculations, which can be used to obtain the relevant activation energies. For example, Linic and Bartea have shown that a mean-field kinetic model of the selective oxidation of ethylene on an Ag catalyst, developed on the

¹Center for Atomic-Scale Materials Physics, ²Department of Physics, ³Department of Chemistry, Technical University of Denmark, DK-2800 Lyngby, Denmark. ⁴Haldor Topsøe A/S, Nymøllevej 55, DK-2800 Lyngby, Denmark.

*To whom correspondence should be addressed.
E-mail: norskov@fysik.dtu.dk

activation barriers and stabilities of intermediates for a series of different catalysts are combined with a simple microkinetic model (21). Our work here represents the final step in a complete first-principles description of the Ru-catalyzed NH_3 synthesis.

The starting point for our calculation is the potential energy diagram for the full reaction (20) (Fig. 1). The calculations (22) show that step sites are much more reactive for N_2 dissociation than the close-packed (001) surface, a finding that has been verified experimentally (23). By combining the results for step sites in Fig. 1 with harmonic transition state theory, we have shown that N_2 dissociation is by far the slowest step under all realistic reaction conditions (20). We will exploit these findings by treating N_2 dissociation as rate-limiting, and we only consider dissociation along step sites where the active (B_5) sites exist (23).

The results shown in Fig. 1 are for a low coverage of adsorbates. In reality, there will be other atoms and molecules adsorbed in the vicinity of the reacting molecule, and the activation energy for dissociation, $E_{\text{a},i}$, and thus the rate constant, $k_i = v e^{-E_{\text{a},i}/kT}$ where v is the prefactor, k is the Boltzmann constant, and T is the temperature, will depend on the local environment (Fig. 2). Each local environment i will contribute to the total rate with a weight given by the probability P_i of finding this environment. The total rate r can be written as

$$r(T, p_{\text{N}_2}, p_{\text{H}_2}, p_{\text{NH}_3}) =$$

$$(1 - \frac{p_{\text{NH}_3}^2}{p_{\text{H}_2}^3 p_{\text{N}_2} K_g}) \sum_i P_i k_i p_{\text{N}_2}$$

where K_g is the gas-phase equilibrium constant, and p_{N_2} , p_{H_2} , and p_{NH_3} are the pressures of N_2 , H_2 , and NH_3 , respectively. The $(1 - \frac{p_{\text{NH}_3}^2}{p_{\text{H}_2}^3 p_{\text{N}_2} K_g})$ term ensures that the gas phase equilibrium is established.

The probability P_i is given by the equilibrium between H_2 and NH_3 in the gas phase and adsorbed H , N , NH , NH_2 , and NH_3 ; all of the steps after the rate-limiting N_2 dissociation (Fig. 1) are in equilibrium. For this reason, we calculated the free energy of adsorption for all of the adsorbates. The entropy contributions were calculated on the basis of a complete normal mode analysis with the harmonic approximation (table S2) (22). We also calculated all possible nearest-neighbor interactions along the step (table S3). In principle, all of the interactions on the lower step should also be included. However, because we found that only H atoms appeared on the lower step, only the $\text{H}-\text{H}$ interaction was needed. The use of grand canonical Monte Carlo simulations provides ensembles of the system in equilibrium and thus the probabilities P_i . Because N_2 dissociates with one N atom at the top of the step

and another at the bottom, an environment i is defined by having an empty site at the upper and lower step sites simultaneously and by the occupancy of the four neighboring sites.

In order to test the predictions of the rate for a real catalyst under industrially relevant conditions, we measured the activity for a Ru catalyst supported on magnesium aluminum spinel that contained 11.1 weight percent (wt %) Ru (24). The experimental results are in the form of the NH_3 productivity from a plug flow reactor loaded with a catalyst containing 0.2 g of the 11.1 wt % Ru/MgAl₂O₄ catalyst as a function of the input partial pressures, the flow, and the temperature. We integrated the NH_3 synthesis rate down through the reactor in order to obtain the calculated NH_3 productivity.

The only information about the catalyst we needed in order to compare calculations to

experiments is the number of active sites per gram of catalyst. Thus, we characterized the activated catalyst by TEM, and we obtained the particle size distribution by analyzing $\sim 10^3$ particles. The active-site density is not directly given by the particle size distribution, because only the B_5 sites are active for N_2 dissociation. Steps can be clearly observed in the TEM image of the Ru particle (Fig. 3), but it is not possible to count them. To estimate the fraction of B_5 sites as a function of particle size, we calculated the surface energy of all the low-energy facets of Ru and used them in a Wulff construction to give the basic particle shape. From DFT calculations, we found that the (001)/(101) edges lower their energy by a reconstruction in which the edge row of atoms is removed. This process gives rise to the steps that contain B_5 sites along the edge.

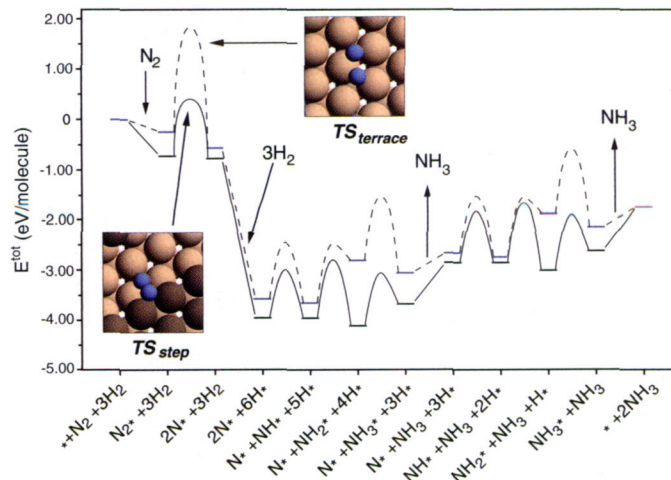


Fig. 1. The calculated potential energy (E_{tot}) diagram for NH_3 synthesis from N_2 and H_2 over close-packed (001) and stepped Ru surfaces (20). A * denotes an empty site and X^* an adsorbed species. The configuration of the transition states (TS) for N_2 dissociation over the terrace and step sites is shown in the insets.

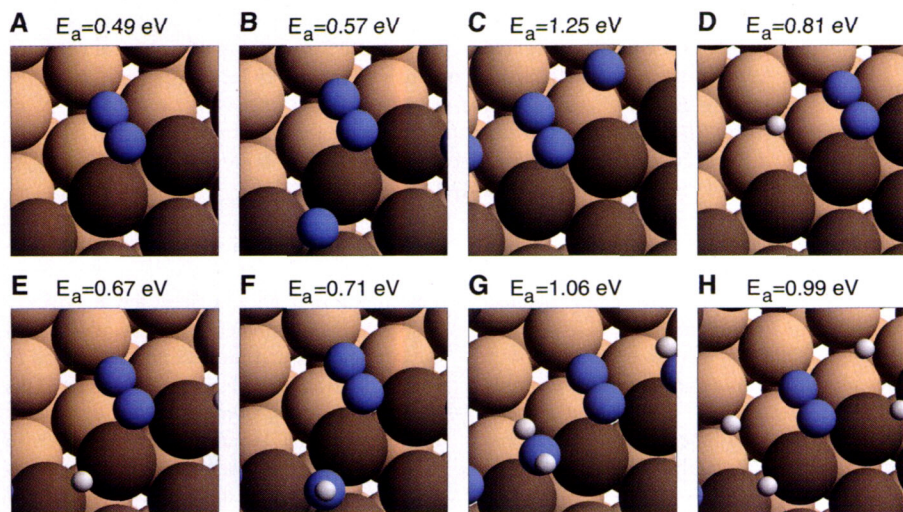


Fig. 2. Calculated activation energies (E_a) and transition state configurations for different local environments. A B_5 site is shown with (A) no adsorbates in the neighboring sites, (B) adsorbed N on the upper step, (C) adsorbed N on the lower step, (D) adsorbed H on the lower step, (E) adsorbed H on the upper step, (F) adsorbed NH on the upper step, (G) adsorbed NH_2 on the upper step, and (H) adsorbed H on both the upper and lower steps. N atoms are shown in blue, H in white, and Ru in light and dark brown.

Our estimate of the particle morphology is quite crude, and it neglects the interaction with the support and changes in the surface energies caused by adsorption. However, the shape is similar to that found in the TEM image, and the fraction of B_5 (step) sites was insensitive to such details. The lack of active sites on the smallest Ru particles is in full

agreement with an experimental observation that the activity of a Ru catalyst can increase as a result of sintering the smallest Ru particles in a supported catalyst (25). The active-site density could now be calculated, and by folding it with the measured size distribution, we obtained the number of active sites per Ru mass. The largest uncertainty in

this estimate is the implicit assumption that the Wulff polyhedra are complete, i.e., that there are no partly filled layers. Our estimate is likely a lower bound to the number of active sites.

A direct comparison of the calculated and measured NH_3 productivity at a number of different conditions is shown in Fig. 4A. Given that there are no fitted parameters, the agreement is excellent. The overall rate is too small by a factor of ~3 to 20, and there is a tendency for the calculated inhibition by NH_3 to be slightly too weak.

The calculations provide insight into the exact nature of the active sites for the NH_3 synthesis reaction over Ru. In Fig. 4B, we give results that show the local environments contributing to the synthesis in one specific slice of the reactor. The largest contribution to the total rate does not come from the local environment with the lowest activation energy (Fig. 2). The state of the surface during synthesis conditions is such that the configuration with adsorbed H on the upper step dominates the total rate.

The agreement between theory and experiment in Fig. 4A might seem surprising, considering that the inherent accuracy of the DFT calculations is of the order 0.2 to 0.3 eV (26). An error in an activation energy of 0.25 eV, for instance, gives rise to an error in the rate of an elementary reaction of a factor of 148 at 600 K. The important point is that the total reaction rate is considerably less sensitive to the absolute error than the rate of the individual steps. We tested the sensitivity of the results to the main approximation in the DFT calculations, the exchange correlation energy functional. All of the calculations were done with the RPBE functional (26), but we also calculated all of the parameters using another functional,

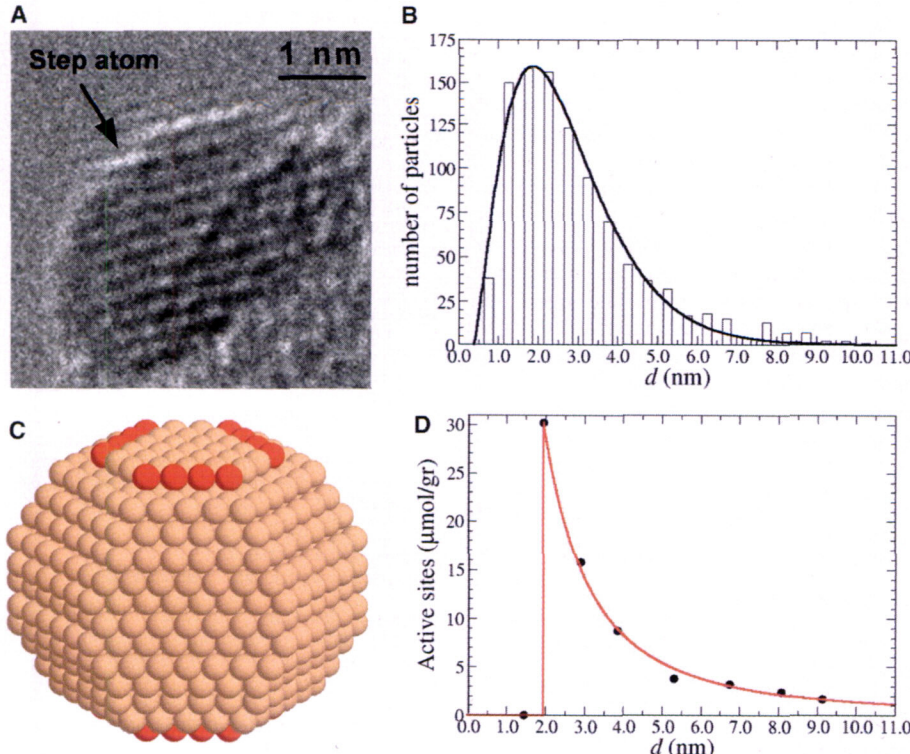


Fig. 3. (A) TEM image of a supported Ru particle with a step. (B) Particle size distribution function obtained from the TEM experiments. d , diameter. (C) A typical calculated Ru particle, with an average diameter of 2.9 nm. Atoms that belong to active B_5 sites are shown in red. (D) Density of active sites as a function of particle diameter, as calculated through analysis of the atomistic Wulff construction.

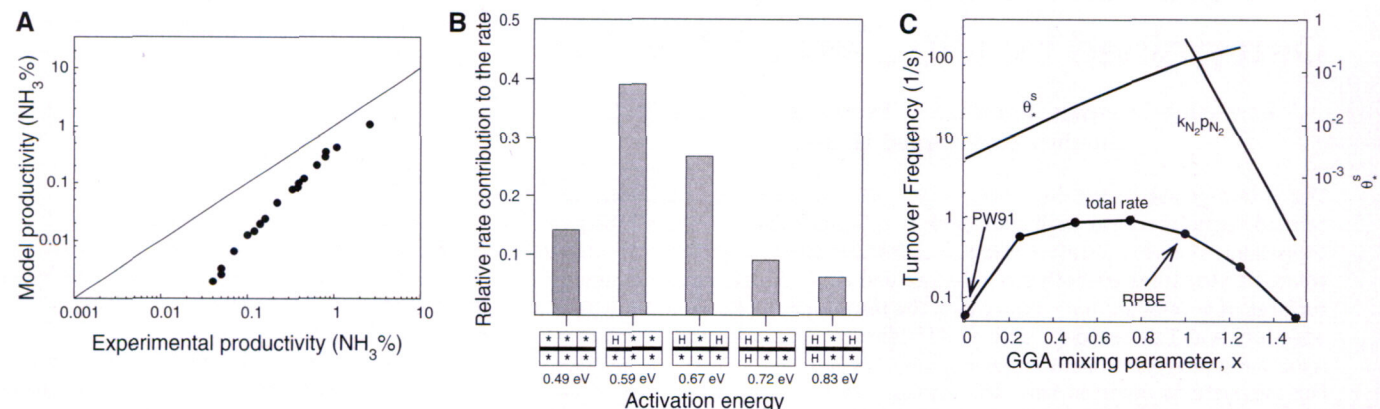


Fig. 4. (A) Comparison of the ammonia productivity from the model with experimental results. Complete agreement would mean that the results should follow the diagonal line. The total pressure was 100 bar; the ratio of N_2 to H_2 was 1:3; the total flow range over 0.2 g of catalyst was between 40 to 267 ml/min (standard temperature and pressure); the conversion range was ~0 to 20% of equilibrium; and the temperature range was from 320°C to 440°C. (B) The relative contributions to the rate in one slice of the reactor. On the x axis, we use a symbolic representation of the local environment,

showing the dissociation sites and four neighboring sites on the upper and lower steps. (C) Dependence of the rate on a parameter x that determines the mixing of results obtained by two different treatments of exchange-correlation effects, the generalized gradient approximation (GGA) PW91 and RPBE methods. The variation in the rate for N_2 dissociation on free sites, $p_{N_2}k_{N_2}$, and the coverage of free sites at the step, θ_s^* , are also given, showing why large variations in both compensate to give a small variation in the total rate that is proportional to both $p_{N_2}k_{N_2}$ and θ_s^* .

PW91 (27). We then interpolated all of the calculated energies between the two: $E(x) = xE_{\text{RPBE}} + (1-x)E_{\text{PW91}}$. The plot of the rate as a function of the mixing parameter x (Fig. 4C) shows a very weak dependence, because there is a compensation effect between the different steps in the total reaction (28). Changing from RPBE to PW91 decreased the barrier for N_2 dissociation substantially (by 0.6 eV) and made the dissociation of N_2 much faster. The dissociative chemisorption energy of H_2 changed simultaneously from -0.36 (RPBE) to -0.52 (PW91) eV, and the N_2 chemisorption energy changed from -0.8 (RPBE) to -1.4 (PW91) eV. These changes increased the coverage (through the equilibrium with H_2 and NH_3 in the gas phase) and decreased the number of free sites for dissociation. Because the barrier for dissociation and the stability of the intermediates on the surface vary together, a change in the overall interaction strength has only a small effect on the net rate. It is this compensation between two opposite trends that gives rise to a volcano in the catalytic activity as a function of the bond strength (28). The compensation effect is largest near to the maximum of the volcano (that is, for the best catalysts).

The insensitivity of the total catalytic rate to errors in the overall adsorption energies raises the question of the origin of the remaining discrepancy between the measured and calculated results (Fig. 4A). One possibility is that the number of active sites is underestimated. Another possible source of discrepancy could be systematic errors in the

description of the difference in bonding of different adsorbates or configurations. We tested the sensitivity of the results to such relative errors by decreasing the stability of adsorbed H relative to the NH_x species by 0.06 eV. It turns out that this is enough to make the calculated points match the measured ones completely at all temperatures and flows. Small relative errors are therefore a likely source of the underestimate of the rate in Fig. 4A. By the same token, the ability of the calculations to predict the absolute rate to within a factor of 3 to 20 suggests that the relative errors are only of the order 0.06 eV ($\sim kT$ at reaction conditions) for the exchange correlation functional used here.

Colinear variations in activation energies and bond strengths are found quite generally (21), so we would expect compensation effects to be found for other reactions. This built-in insensitivity to absolute errors, together with the higher accuracy of the DFT methods for relative energies, offers hope that DFT calculations can give a good overall description of the catalytic activity of other reactions as well.

References and Notes

- S. Linic, M. A. Bartea, *J. Am. Chem. Soc.* **125**, 4034 (2003).
- K. Reuter, D. Frenkel, M. Scheffler, *Phys. Rev. Lett.* **93**, 116105 (2004).
- M. Boudart, *Top. Catal.* **1**, 405 (1994).
- F. Haber, Nobel Prize Lecture 1918, in *Nobel Lectures, Chemistry 1901–1921* (Elsevier, Amsterdam, 1966).
- C. Bosch, Nobel Prize Lecture 1931, in *Nobel Lectures, Chemistry 1922–1941* (Elsevier, Amsterdam, 1966).
- A. Mittasch, *Adv. Catal.* **2**, 81 (1950).

- P. H. Emmett, S. Brunauer, *J. Am. Chem. Soc.* **55**, 1738 (1933).
- P. H. Emmett, S. Brunauer, *J. Am. Chem. Soc.* **56**, 35 (1934).
- F. Boszo, G. Ertl, M. Grunze, M. Weiss, *J. Catal.* **49**, 18 (1977).
- G. Ertl, M. Weiss, S. B. Lee, *Chem. Phys. Lett.* **60**, 391 (1979).
- Z. Paal, G. Ertl, S. B. Lee, *Appl. Surf. Sci.* **8**, 231 (1981).
- G. Ertl, S. B. Lee, M. Weiss, *Surf. Sci.* **114**, 527 (1982).
- G. Ertl, *J. Vac. Sci. Technol. A* **1**, 1247 (1983).
- N. D. Spencer, R. C. Schoonmaker, G. A. Somorjai, *J. Catal.* **74**, 129 (1982).
- D. R. Strongin, J. Carranza, S. R. Bare, G. A. Somorjai, *J. Catal.* **103**, 213 (1987).
- D. R. Strongin, G. A. Somorjai, *J. Catal.* **109**, 51 (1988).
- P. Stoltze, J. K. Nørskov, *Phys. Rev. Lett.* **55**, 2502 (1985).
- J. A. Dumesic, A. A. Triviño, *J. Catal.* **116**, 119 (1989).
- M. Bowker, *Top. Catal.* **1**, 165 (1994).
- A. Logadottir, J. K. Nørskov, *J. Catal.* **220**, 273 (2003).
- A. Logadottir et al., *J. Catal.* **197**, 229 (2001).
- Materials and methods are available as supporting material on *Science Online*.
- S. Dahl et al., *Phys. Rev. Lett.* **83**, 1814 (1999).
- S. Dahl, J. Sehested, C. J. H. Jacobsen, E. Törnqvist, I. Chorkendorff, *J. Catal.* **192**, 391 (2000).
- C. J. H. Jacobsen et al., *J. Mol. Catal. A* **163**, 19 (2000).
- B. Hammer, L. B. Hansen, J. K. Nørskov, *Phys. Rev. B* **59**, 7413 (1999).
- J. P. Perdew et al., *Phys. Rev. B* **46**, 6671 (1992).
- T. Bligaard et al., *J. Phys. Chem. B* **107**, 9325 (2003).
- We thank the Danish Center for Scientific Computing for computer resources. Supported by EU project no. HPRN-CT-2002-00170.

Supporting Online Material

www.sciencemag.org/cgi/content/full/307/5709/555/DC1

Materials and Methods

Figs. S1 to S6

Tables S1 to S4

References and Notes

15 October 2004; accepted 17 December 2004
10.1126/science.1106435

Dark Structures in Molecular Radiationless Transitions Determined by Ultrafast Diffraction

Ramesh Srinivasan, Jonathan S. Feenstra, Sang Tae Park,
Shoujun Xu,* Ahmed H. Zewail†

The intermediate structures formed through radiationless transitions are termed "dark" because their existence is inferred indirectly from radiative transitions. We used ultrafast electron diffraction to directly determine these transient structures on both ground-state and excited-state potential energy surfaces of several aromatic molecules. The resolution in space and time (0.01 angstrom and 1 picosecond) enables differentiation between competing nonradiative pathways of bond breaking, vibronic coupling, and spin transition. For the systems reported here, the results reveal unexpected dynamical behavior. The observed ring opening of the structure depends on molecular substituents. This, together with the parallel bifurcation into physical and chemical channels, redefines structural dynamics of the energy landscape in radiationless processes.

Radiationless transitions abound in chemical, physical, and biological systems, yielding such diverse phenomena as the conversion

of radiation to heat and the photodamage and photocarcinogenesis of DNA (1–5). After light absorption, a molecule can undergo ra-

diationless processes of two general types: photochemical, involving bond fragmentation or isomerization; and photophysical, involving transitions between electronic states while either conserving spin (internal conversion) or altering spin (intersystem crossing). For more than eight decades [(6) and references therein], our understanding of such radiationless processes has come from indirect evidence based on yields and decay rates of the radiative population. Theoretical studies have in turn advanced the concepts of a "heat bath" within the molecule (originally thought to violate the rules of quantum mechanics) and of conical intersections in the energy landscape (7–9).

Experimentally, the presence of nonradiative electronic relaxation processes was first deduced from the decrease in steady-state emission quantum yield of molecules at low pressures (10). With the advent of picosecond time resolution, it became possible to study the time scale of these processes [(11) and references therein]; with femtosecond time resolution, the actual nuclear motions were resolved [(12) and references